

INTRODUCTORY OVERVIEW OF EULERIAN & LAGRANGIAN PERTURBATION THEORIES

F. R. BOUCHET

Institut d'Astrophysique de Paris, CNRS, 98bis Boulevard Arago, F-75014 Paris
France.

Contents

1	THE FLUID EQUATIONS	2
1.1	Microscopic Description	2
1.2	Macroscopic Description	3
1.3	Velocity Moments and the Fluid Limit	3
2	EULERIAN PERTURBATIVE SOLUTIONS	4
2.1	Linear Density Field	4
2.2	Linear Peculiar Velocity Field	6
2.3	Non-Linear Corrections	7
3	SOME BASIC APPLICATIONS	8
3.1	The PDF as a Measure of Large Scale Structures	8
3.2	Moments of the PDF	9
3.3	Edgeworth Expansion of the PDF	12
3.4	Validity of Perturbation Theory	13
4	FURTHER DEVELOPMENTS	15
4.1	Higher Order Moments	15
4.2	Higher Order Corrections to the Moments	15
4.3	General Initial Conditions	16
4.4	Biasing and comparisons to data	16
5	ZELDOVICH APPROXIMATION	18
5.1	Derivation from Eulerian Theory	18
5.2	Galactic Spin Origin	19
5.3	Density Contrast & Pancakes	19
6	LAGRANGIAN PERTURBATION THEORY	20
6.1	Perturbative equations	21
6.2	Low order Solutions	22
7	APPLICATIONS	24
7.1	Moments in the Lagrangian approach	24
7.2	Redshift Space Skewness	25
7.3	Approach of the Non-Linear Regime	26
8	CONCLUSIONS	27

These lectures notes give an introduction to the fast developing area of research dealing with perturbative descriptions of the gravitational instability in an expanding universe. I just sketch the outlines of some proofs, and many important contributions

(and references) were left out. Many untouched aspects are reviewed in [44] which also contains a useful reference list.

In the notes dedicated to the Eulerian approach (§1 - §4), I derive the fluid equations starting from a microscopic description, I give their linear solution and some higher order corrections, and describe a number of applications concerning the evolution of the one point probability density function for the density contrast field and for the divergence of the corresponding velocity field.

In the notes dedicated to the Lagrangian point of view (§5 - §7), I recall Zeldovich Approximation and its higher orders corrections, and present some applications, like their use in describing the statistical effect of the real space-redshift mapping, or as approximate description of the full non-linear dynamics.

1. THE FLUID EQUATIONS

In this section, I derive the fluid equations as velocity moments of the full microscopic evolution equations taken in the mean field, or continuum, limit. We shall restrain to the case of perturbations which may be described in the Newtonian approximation.

In all the following, we use comoving coordinates $\mathbf{r} = a\mathbf{x}$, and $\mathbf{p} = ma^2\partial_t\mathbf{x}$, where m stands for the particles mass, and a for the metrics scale or expansion factor. In that case, the motion and field (Poisson) equations write

$$\partial_t\mathbf{p} = -\nabla\phi, \quad \nabla^2\phi = 4\pi Ga^2\bar{\rho}\delta,$$

if $\delta \equiv \rho/\bar{\rho} - 1$ stands for the density contrast field. The solution to Poisson equation is $\phi(x) = -Ga^2 \int d\mathbf{x}'(\rho(\mathbf{x}') - \rho_b)/|\mathbf{x}' - \mathbf{x}|$, where $\rho(\mathbf{x}')$ fluctuates in an homogeneous and isotropic way around the background value ρ_b . Thus

$$-\nabla\phi = Ga^2 \int (\rho(\mathbf{x}') - \rho_b) \frac{\mathbf{x}' - \mathbf{x}}{|\mathbf{x}' - \mathbf{x}|} d\mathbf{x}' = Ga^2 \int \rho(\mathbf{x}') \frac{\mathbf{x}' - \mathbf{x}}{|\mathbf{x}' - \mathbf{x}|} d\mathbf{x}'$$

where it is implicit that, in the last integral, one follows the prescription of integrating first over angle and only then over \mathbf{x}' .

1.1. Microscopic Description

Let us denote by $f(\mathbf{x}, \mathbf{p}, t)$ the one-particle distribution function, i.e. the probability density of finding at time t a *collisionless* particle within the infinitesimal phase space volume $d\mu = d\mathbf{x}d\mathbf{p}$. For N_p point particles, each with a trajectory given by $\mathbf{x}_i(t)$ and $\mathbf{p}_i(t)$, the system is fully described by

$$f(\mathbf{x}, \mathbf{p}, t) = \sum_{i=1}^{N_p} \delta_D(\mathbf{x} - \mathbf{x}_i(t)) \delta_D(\mathbf{p} - \mathbf{p}_i(t)),$$

where δ_D stands for Dirac's function. Particle conservation plus Liouville theorem (i.e. $\frac{d\mu}{dt} = 0$) give the equation governing the evolution of the system, $\frac{df}{dt} = 0$.

In our discrete particle model, the density is

$$\rho = \rho_b[1 + \delta(\mathbf{x}, t)] = \frac{m}{a^3} \int f(\mathbf{x}, \mathbf{p}, t) \mathbf{p} = \frac{m}{a^3} \sum_i \delta_D(\mathbf{x} - \mathbf{x}_i),$$

and one recovers the familiar form $-\nabla\phi = Ga^2 \sum_i \frac{\mathbf{x}_i - \mathbf{x}}{|\mathbf{x}_i - \mathbf{x}|^3}$. By using the motion equation, we then get the *Klimontovich equation*

$$d_t f + \frac{\mathbf{p}}{ma^2} \cdot \nabla_x f - m \nabla\phi \cdot \nabla_p f = 0,$$

a complete description with the field equation

$$-m\nabla\phi = \frac{Ga^2}{a} \int f(\mathbf{x}', \mathbf{p}', t) \frac{\mathbf{x}' - \mathbf{x}}{|\mathbf{x}' - \mathbf{x}|^3} d\mathbf{x}' d\mathbf{p}'.$$

1.2. Macroscopic Description

Let us now consider a smoothed out (phase space) density obtained by averaging over patches of size intermediate between the microscopic level and the system size, so that we can take “local” averages. In this “coarse-grain” distribution, we lose the discrete character of the particles. This can also be seen as a continuum (or thermodynamical) limit such that one formally takes the limit of an infinite number of particles, $N_p \rightarrow \infty$, while their individual mass goes to zero, $m \rightarrow 0$, keeping the mass density $N_p m$ constant.

In this *mean field* limit, the Klimontovich equation becomes the *Vlasov equation*. It has formally the same writing, but now the solutions f are to be found in the ensemble of smooth, continuous, functions (since the discrete character embodied by Dirac function has been lost). Note that by losing the discrete character of the particles, one of course cannot describe the effect of direct encounters (e.g. two-relaxation effects). In other words, one only considers the evolution of perturbations through *fluctuations of the mean field* created collectively by many particles.

Intuitively, this collective description of the evolution should be legitimate when the 2-body potential energy at the mean interparticle distance $n^{-1/3}$, $Gm^2 n^{1/3}$, is much smaller than their average kinetic energy, $m\sigma_v^2$, which is indeed confirmed by more rigorous analysis.

1.3. Velocity Moments and the Fluid Limit

A classical method amounts to find equations between various velocity (momentum) moments of the one-point distribution function $f(\mathbf{x}, \mathbf{p}, t)$. These are simply obtained by multiplying the equation governing the evolution of f (here the Vlasov equation) by products of velocity components (or here momentum components p^α) before integrating over all the velocities components.

The zeroth moment relates the density $\rho(x) = (m/a^3) \int \mathbf{p} f(\mathbf{x}, \mathbf{p}, t)$ to the mean velocity of a phase space element, $\mathbf{v} = \langle \mathbf{p}/ma \rangle = \int (\mathbf{p}/ma) f d\mathbf{p} / \int f d\mathbf{p}$ by the *continuity equation*

$$\partial_t \rho + 3 \frac{\dot{a}}{a} \rho + \frac{1}{a} \nabla \cdot \rho \mathbf{v} = 0, \quad (1)$$

which is often rewritten as $\partial_t \delta + \frac{1}{a} \nabla \cdot [(1 + \delta) \mathbf{v}] = 0$.

The first moment obtains by multiplying Vlasov equation by the α component of momentum, p^α , which yields the velocity equation

$$\partial_t \int p^\alpha d\mathbf{p} + \frac{1}{a^2} \partial_\beta \int p^\alpha p^\beta f d\mathbf{p} + a^3 \rho \partial_\alpha \phi = 0. \quad (2)$$

It is then convenient to introduce the *centered* second moment tensor, i.e. the “pressure tensor”, $P^{\alpha\beta}$, defined by

$$\left\langle \frac{p^\alpha p^\beta}{ma ma} \right\rangle = \frac{P^{\alpha\beta}}{\rho} + v^\alpha v^\beta,$$

to rewrite the source term in the mean velocity equation (2).

Truncating the hierarchy: the second moment equation would in turn relate the pressure tensor to a “heat flux tensor” $\langle p^\alpha p^\beta p^\gamma \rangle$. Of course, one obtains by this procedure a hierarchy of equations, each relating the evolution of a moment to the one of next higher order.

Truncating the hierarchy amounts to impose a relation between a given moment and the lower ones. In particular, one often assumes an isotropic pressure tensor

$$\frac{P^{\alpha\beta}}{\rho} = \delta_{\alpha\beta} \frac{p}{\rho},$$

where $\delta_{\alpha\beta}$ is Kronecker’s symbol, and p is the usual pressure. In that case the first moment equation (2) becomes the *Euler equation*

$$\partial_t v^\alpha + \frac{\dot{a}}{a} v^\alpha + \frac{(\mathbf{v} \cdot \nabla) v^\alpha}{a} = -\frac{\partial_\alpha p}{a\rho} - \frac{\partial_\alpha \phi}{a},$$

which together with the continuity equation and an equation of state relating the pressure and the density forms a closed system of equation, often referred to as the “fluid equations”.

Note though that till now we have said nothing about the role of “collisions”. And indeed, particles interacting only gravitationally like neutrinos should have an isotropic velocity dispersion everywhere, as long as one does not reach the multi-stream regime, i.e. before “shell crossing”. In fact, early on, the velocity dispersion can often be neglected altogether, $p = 0$, and the equations above describe a so-called “dust universe”. But of course, one expects on very general grounds (see the Lagrangian section for more details) to have an anisotropic, “pancake-like” collapse, which cannot be followed any more by these equations (although one may attempt to guess an “effective” equation of state mimicking macroscopically the complex microscopic dynamics).

On the other hand, if we have a *bona fide* fluid made of baryons, their collective interactions do maintain a local isotropy and establish an equation of state, with e.g. $p(\rho) = p(\rho_b) + c_s^2 \rho_b \delta$, where c_s stands for the sound speed, $c_s = (dp/d\rho)^{1/2}$. In any case, the point is that the “fluid equations” can properly be used to describe (some of) the evolution of dark matter collisionless particles.

Other forms of the continuity and Euler equations: it is often convenient to introduce the conformal time τ defined by $d\tau = dt/a$. Denoting the partial derivative versus τ by an overdot, and redefining \mathbf{v} as $\dot{\mathbf{x}}$, the previous equations become

$$\dot{\delta} + \nabla \cdot [(1 + \delta)\mathbf{v}] = 0 \quad \text{and} \quad \dot{\mathbf{v}} + \frac{\dot{a}}{a} \mathbf{v} + (\mathbf{v} \cdot \nabla)\mathbf{v} = -\frac{\nabla p}{\rho} - \nabla \phi. \quad (3)$$

Finally, it is advantageous for some applications to rather introduce $D(t)$ as the time coordinate, $D(t)$ standing for the linear growth rate of density fluctuations (see below).

2. EULERIAN PERTURBATIVE SOLUTIONS

2.1. Linear Density Field

By inserting the first moment equation (2) into the continuity equation (1) one gets

$$\partial_t^2 \delta + 2\frac{\dot{a}}{a} \partial_t \delta = \frac{1}{a^2} \nabla \cdot [(1 + \delta)\nabla \phi] + \frac{1}{a^2} \partial_\alpha \partial_\beta \left[\frac{P^{\alpha\beta}}{\rho_b} + (1 + \delta)v^\alpha v^\beta \right]. \quad (4)$$

The Eulerian perturbative regime is when

$$\delta \ll 1 \quad \text{and} \quad \left(\frac{vt}{d}\right)^2 \sim \delta \ll 1,$$

where d stands for the coherence length of the perturbation and t its dynamical time, $t \sim (G\rho)^{-1/2}$ (in an $\Omega = 1$ universe, the FRW equations lead to $6\pi G\rho t^2 = 1$ in the matter era). The second requirement is simply that gradients should be small. In *linear* perturbation theory, one neglects all term in $\delta^2, v^2, \delta v$, and the fluid equations assume the form

$$\partial_t \delta + \nabla \cdot \mathbf{v} a = 0 \quad \text{and} \quad \partial_t^2 \delta + 2\frac{\dot{a}}{a} \partial_t \delta = \frac{\nabla^2 p}{\rho_b a^2} + 4\pi G \rho_b \delta. \quad (5)$$

Solutions are known for many different cases, i.e. for different equation of state, and different time evolution of the factor of expansion a . Here we recall some of the most useful ones.

2.1.1. Dust Universe, $p = 0$: since there are now no spatial derivatives in the equations, the evolution is self-similar for arbitrary density contrasts δ . Let us denote by D_a and D_b the two growth rates solution of the second order differential equation, and by A and B the associated spatial parts, so that the solution if the linear combination

$$\delta(\mathbf{x}, t) = A(\mathbf{x})D_a(t) + B(\mathbf{x})D_b(t),$$

D_a corresponding by convention to the fastest growing mode

In the Einstein-de Sitter case, $\Omega = 1$ and $a \propto t^{2/3}$. Thus eq. (4) becomes $\partial_t^2 \delta + \frac{4}{3t} \partial_t \delta = \frac{2}{3t^2} \delta$, and we have $D_a = t^{2/3}$ and $D_b = t^{-1}$. Note that the exponential growth of a static universe (when $\dot{a} = 0$) is now much slower.

In the open case, full solution may be obtained by changing the time coordinate to a given by

$$\left(\frac{\dot{a}}{a}\right)^2 = \frac{8\pi G \rho_b}{3} \left[1 + (\Omega_0^{-1} - 1) \left(\frac{a}{a_0}\right)\right].$$

But in the asymptotically late regime when the curvature term dominates, i.e. $a \propto t$, one simply has $\partial_t^2 \delta + \frac{2}{t} \partial_t \delta + \frac{3\Omega}{2t^2} \delta \sim \partial_t^2 \delta + \frac{2}{t} \partial_t \delta = 0$, since $4\pi G \rho_b \ll t^{-2}$. Thus $D_a = 1$ and $D_b = t^{-1}$; At best the density contrast is frozen in the free expansion regime. And this happens when $(\Omega_0^{-1} - 1)a/a_0 \sim 1$, i.e when $1 + z_{freeze} = \Omega_0^{-1} - 1$. In other words, a perturbation grows like $t^{2/3}$ at $z \gg z_{freeze}$ and stops afterwards.

Fixing $A(\mathbf{x})$ and $B(\mathbf{x})$: the solution to our second order differential equation is fully specified by giving, e.g. the initial density contrast δ_i and velocity \mathbf{v}_i at time t_i ,

$$\delta_i = AD_a(t_i) + BD_b(t_i), \quad \text{and} \quad -\frac{\nabla \cdot \mathbf{v}_i}{a_i} = A \left. \frac{dD_a}{dt} \right|_i + B \left. \frac{dD_b}{dt} \right|_i.$$

Introducing the Wronskian $W = D_a(t_i) \left. \frac{dD_b}{dt} \right|_i - D_b(t_i) \left. \frac{dD_a}{dt} \right|_i$, we have then

$$\delta = \frac{\delta_i}{W} \left[D_a \left. \frac{dD_b}{dt} \right|_i - D_b \left. \frac{dD_a}{dt} \right|_i \right] + \frac{\nabla \cdot \mathbf{v}_i}{a_i} [D_a D_b(t_i) - D_b D_a(t_i)].$$

In the Einstein-de Sitter case, $W = -\frac{5}{3}\frac{D_a(t_i)D_b(t_i)}{t_i}$. If the initial velocity may be neglected, one then finds

$$\delta = \delta_i \left[\frac{3}{5}D_a + \frac{2}{5}D_b \right],$$

with $\delta = \frac{3}{5}D_a\delta_i$ at late times (in the following, we shall drop the subscript a , and D will refer to the fastest growth rate). On the other hand, in numerical simulations, one usually sets the velocity field to select the growing mode only.

2.1.2. Jeans length of an ideal fluid with $p = p(\rho)$: plugging $p(\rho) = p(\rho_b) + c_s^2\rho_b\delta$ in (5), we get

$$\partial_t^2\delta + 2\frac{\dot{a}}{a}\partial_t\delta = \left(\frac{c_s}{a}\right)^2\nabla^2\delta + 4\pi G\rho_b\delta.$$

It's Fourier transform is

$$\partial_t^2\delta_k + 2\frac{\dot{a}}{a}\partial_t\delta_k = \left[4\pi G\rho_b - \frac{c_s^2k^2}{a^2}\right]\delta_k,$$

which shows that there is a characteristic wavelength $\lambda_J = 2\pi/k_J = \pi\frac{c_s}{G\rho} \sim c_s t$ for the scale of a perturbation. Above this Jeans length, the pressure cannot counteract the self-gravity of the perturbation ($c_s t < \lambda$), while at $\lambda < \lambda_J$ the perturbation oscillates like a sound wave.

2.2. Linear Peculiar Velocity Field

2.2.1. Solution in a dust Universe: the linearized continuity and velocity equation in the pressureless case reduce to

$$\partial_t\delta + \frac{1}{a}\nabla\mathbf{v} = 0 \quad \text{and} \quad \partial_t\mathbf{v} + \frac{\dot{a}}{a}\mathbf{v} = -\frac{\nabla\phi}{a}.$$

Since $\delta \propto D$, we have $\nabla \cdot \mathbf{v} = a\partial_t\delta = -Haf\delta = -\frac{Haf}{4\pi G\rho_b a^2}\nabla^2\phi$ where H stands for Hubble's "constant", \dot{a}/a , and $f(\Omega) = (a/D)dD/da$ can be well fitted by $\Omega^{0.6}$ over a large range. Thus

$$\mathbf{v} = \frac{2}{3}\frac{f}{H\Omega}\frac{-\nabla\phi}{a} + \frac{\nabla \times U(\mathbf{x})}{a},$$

which satisfies the first equation for an arbitrary $U(\mathbf{x})$. This last term decays as a^{-1} , as does v in the absence of a driving term. Since it quickly becomes negligible, we find that at the linear order *the velocity is parallel to the acceleration* at late times, the proportionality constant depending rather strongly on the density parameter.

2.2.2. Application to data: the strong Ω dependence of $f(\Omega)$ has been used in the context of the linear bias model, in which one assumes that, at least on sufficiently large scales, the density contrast field computed from galaxies, δ_g , is simply on average proportional to the underlying density field, i.e. $\delta_g = b\delta$ (although that may turn out to be a poor approximation for some applications). In that case, the velocity field is proportional to the parameter $\beta = f(\Omega)/b$. Since one may estimate δ_g through

$$1 + \delta_g = \frac{1}{n} \sum_i \frac{1}{\Phi(\mathbf{x}_i)} \delta_D(\mathbf{x} - \mathbf{x}_i) \quad \text{with} \quad n = \frac{1}{V} \sum_i \frac{1}{\Phi(\mathbf{x}_i)},$$

where the density $n = \frac{1}{V} \sum_i \frac{1}{\Phi(\mathbf{x}_i)}$ obtains from the catalog selection function Φ , one may then compare the predicted velocity from the observed galaxy density field, \mathbf{v}_{pred} to the ‘‘observed’’ one. One thus try to find the β which best match the two velocity fields, with

$$\mathbf{v}_{pred} = \frac{\beta H a}{4\pi} \int_{x < x_{max}} \delta_g(\mathbf{x}') W(|\mathbf{x}' - \mathbf{x}|) \frac{\mathbf{x}' - \mathbf{x}}{|\mathbf{x}' - \mathbf{x}|} d^3 x'.$$

Note that in practice, we do not have an infinite catalog, and we have to truncate the integral at a maximal radius x_{max} selected such that the signal still dominates over the shot noise (i.e. beware of $1/\Phi$!). Even worse, not all the sky is surveyed homogeneously and isotropically (e.g. close to the galactic plane), so that the density field has to be extrapolated in some way. Note also the introduction of a window function W (whose size is typically greater than 500 km/s) to average over a rather large volume in order to reduce the level of non-linearities, reduce the shot noise, the distance uncertainties and the impact of the triple-value zone in relating redshifts to distances ($\dot{a}x = cz - v$ is solved iteratively)

Alternatively, one could use the proper velocities of galaxies to compare with the observed density field. This area has been the subject of intense research in the last few year, and will be covered in much greater detail in the notes of A. Dekel (this volume). For a more in-depth view, one could look at the proceedings [16] of the ‘‘Cosmic Velocity Field’’ meeting held in 1993, or the recent review [47].

2.3. Non-Linear Corrections

Let us now come back to the density field equation (4) for a pressureless medium,

$$\partial_t^2 \delta + 2 \frac{\dot{a}}{a} \partial_t \delta = \frac{1}{a^2} \nabla [(1 + \delta) \nabla \phi] + \frac{1}{a^2} \partial_\alpha \partial_\beta [(1 + \delta) v^\alpha v^\beta]. \quad (6)$$

In order to find a description of the evolution which may remain valid longer than the linear one, we write the density contrast and the velocity fields as perturbative expansions

$$\begin{aligned} \delta(\mathbf{x}, t) &= \delta^{(1)}(\mathbf{x}, t) + \delta^{(2)}(\mathbf{x}, t) + \dots, \\ \mathbf{v}(\mathbf{x}, t) &= \mathbf{v}^{(1)}(\mathbf{x}, t) + \mathbf{v}^{(2)}(\mathbf{x}, t) + \dots, \end{aligned}$$

where $\delta^{(1)}(\mathbf{x}, t)$ and $\mathbf{v}^{(1)}(\mathbf{x}, t)$ are the linear terms obtained previously. They are of order $\delta_i \equiv \varepsilon$ (if we write $\delta^{(1)}(\mathbf{x}, t) = \varepsilon(\mathbf{x}) D(t)$, $\mathbf{v}^{(1)\alpha}(\mathbf{x}, t) = (f/H) \partial_\alpha \Phi_i$, if Φ_i stands for the initial potential $\int \frac{d^3 x'}{4\pi |\mathbf{x} - \mathbf{x}'|} \varepsilon(\mathbf{x}')$, and we retain only the fastest growing modes). The next term $\delta^{(2)} = O(\delta^{(1)})^2 = O(\varepsilon^2)$ is a non-linear correction, solution of the equation when only quadratic non-linearities are retained. The source terms are then products of the linear solutions. The resulting second order solution can then be used iteratively to obtain still higher order solutions...

The solution to the equation of order two in ε is

$$\delta^{(2)} = D(t)^2 \left[\frac{2}{3} [1 + \kappa(t)] \varepsilon^2(\mathbf{x}) + \nabla \varepsilon(\mathbf{x}) \cdot \nabla \Delta + \left[\frac{1}{2} - \kappa(t) \right] \mathcal{T}^2 \right], \quad (7)$$

where $\mathcal{T}^2 = \sum_{\alpha, \beta=1}^3 (\mathcal{T}_{\alpha\beta})^2$ is the contraction of the (linear order) tide tensor

$$\mathcal{T}_{\alpha\beta} = \nabla_\alpha \nabla_\beta \Phi_i - \frac{1}{3} \delta_{\alpha\beta} \nabla^2 \Phi_i \quad (8)$$

whose presence can only speed up the collapse. The parameter $\kappa(t)$ is a slowly varying function of cosmological time which is well approximated (Bouchet *et al* 1992) by

$$\kappa \approx \frac{3}{14}\Omega^{-2/63}, \quad (9)$$

in the range $0.05 \leq \Omega \leq 3$ (the accuracy of this approximation is then better than 0.4%). For $\Omega = 0$, $\kappa = \frac{1}{4}$. The exact expression for $\kappa(\Omega)$, valid in the entire range $\Omega \geq 0$, is given in [8]). For $\Omega = 1$, $\kappa = \frac{3}{14}$, and we find

$$\delta = \delta^{(1)} + \frac{5}{7}\delta^{(1)2} - \partial_\alpha \delta^{(1)} \partial_\alpha \Phi_i + \frac{2}{7} \partial_{\alpha\beta} \Phi_i \partial_{\alpha\beta} \Phi_i,$$

the classical Einstein-de Sitter solution (*e.g.*, [43], hereafter LSS, eq. [18.8]).

Vorticity and Shear By taking the curl of Euler equation (3) when the conformal time τ is used, we find that gravity alone cannot generate vorticity. Indeed, introducing $\omega = \nabla \times \mathbf{v}$, we get (an overdot denoting partial derivatives versus τ)

$$\dot{\omega} = \nabla \times (\mathbf{v} \times \omega) - \frac{\dot{a}}{a} \omega \frac{\nabla \rho \times \nabla p}{\rho^2}.$$

Thus $\dot{\omega} = 0$ for a pressureless fluid which is initially vorticity-free. Furthermore, the density field equation (6) for a pressureless medium can be cast in the following form

$$\ddot{\delta} + \frac{\dot{a}}{a} \dot{\delta} = \frac{4}{3} \frac{\dot{\delta}}{1+\delta} + (1+\delta) \left[\sigma_{\alpha\beta} \sigma^{\alpha\beta} - \frac{1}{2} \omega^2 + 4\pi G \rho_b \delta \right],$$

where the velocity shear tensor now has the form $\sigma^{\alpha\beta} = \frac{1}{2} \left[\frac{\partial \dot{\mathbf{x}}^\alpha}{\partial x^\beta} + \frac{\partial \dot{\mathbf{x}}^\beta}{\partial x^\alpha} \right]$. Thus the shear accelerates the collapse, while vorticity slows it down. This is this acceleration, absent at the linear order, that showed up at the second order [eq. (7)] through the (linear) tide tensor ($\mathcal{T}^{\alpha\beta} = \frac{HfD}{4\pi} \sigma^{\alpha\beta} - \frac{\delta_{\alpha\beta}}{3} \frac{\nabla \cdot \mathbf{v}}{a}$). Finally, let us stress that the rate of collapse depends on the three eigenvalues of the tide tensor, which implies that the highest peaks of the density field do not compulsorily collapse first (see §5.3).

3. SOME BASIC APPLICATIONS

3.1. The PDF as a Measure of Large Scale Structures

Many approaches can be used to characterize statistically the observed large scale structures in the Universe. Here we focus on the one-point distribution function, or PDF. Empirically, this approach was first applied by Hubble in 1934 [30]. Let $Q(r)$ be a physical quantity whose value depends on the location. Let $Q_\ell(r)$ be the smoothed value of Q on scale ℓ , *i.e.*, $Q_\ell(r)$ is obtained by convolving the scalar field $Q(r)$ by a smoothing window W_ℓ of characteristic scale ℓ ($Q_\ell(\mathbf{r}) = Q(\mathbf{s}) * W_\ell(\mathbf{r} - \mathbf{s}) = \int d^3s Q(s) W_\ell(r - s)$). The probability that Q_ℓ lies between Q and $Q + dQ$ is $P(Q, \ell) dQ$, P being its PDF.

If $Q \equiv N$ where N is a number of galaxies, and W is a top-hat window, then the PDF gives the probability of finding N galaxies in a sphere (in 3D) of size ℓ . In the following, Q will be either the mass density contrast field $\delta = \rho/\bar{\rho} - 1$, or the divergence of the associated velocity field in units of the Hubble constant, $\theta = \nabla \cdot \mathbf{v}/H$; we will consider the two most commonly used types of windows, a top-hat and a gaussian one.

Later on, we shall discuss the relation of the mass distribution to the distribution of luminous galaxies.

It is frequently assumed that, very early in the history of the Universe, the density contrast $\varepsilon \equiv \delta(t = t_i)$ could be taken as normally distributed, *i.e.*,

$$P(\varepsilon, \ell) \propto \exp \left[-\frac{\varepsilon_\ell^2}{2\sigma_i^2(\ell)} \right],$$

where $\sigma_i^2(\ell) \equiv \langle \varepsilon_\ell^2 \rangle$ stands for the initial variance of the density contrast field smoothed on scale ℓ . It is assumed to be small at all scales, $\sigma_i \ll 1$. The second moment is the only quantity we need to know in order to fully characterize such a field. Indeed all odd moments of a gaussian PDF are zero, while the $2n$ -th moments are proportional to the n -th power of the variance, $\langle \varepsilon^{2n} \rangle \propto \sigma_i^{2n}$ (the corresponding specification in Fourier space is given in (13)). In the following, we shall refer to such a state as gaussian initial conditions.

Our goal now will be to derive the properties of the PDF today, under the assumption of a time-evolution under the sole influence of the gravitational instability acting on gaussian initial conditions. Under the influence of gravity, underdense regions become even more underdense (although not indefinitely, since the density is bounded from below), while positive density enhancements tend to grow without bound. Clearly the symmetry of the distribution cannot be maintained, and the PDF becomes skewed, *i.e.*, $\langle \delta^3 \rangle$ departs from zero. The distribution also develops a non-zero kurtosis $\langle \delta^4 \rangle - 3\langle \delta^2 \rangle^2$. In the limit of a small variance, $\langle \delta^2 \rangle \ll 1$, the development of skewness and kurtosis are the most important effects. We shall concentrate on those first.

3.2. Moments of the PDF

3.2.1. Skewness of the Unsmoothed Density field: by using the perturbative results in the weakly-nonlinear regime, we can calculate the gravitationally induced skewness under the assumption that ε is a random gaussian field. The lowest order terms in the series for $\langle \delta^3 \rangle$ are

$$\langle \delta^3 \rangle = \langle \delta^{(1)3} \rangle + \langle 3\delta^{(1)2}\delta^{(2)} \rangle + O(\varepsilon^5). \quad (10)$$

The linear solution implies that the first term is $D(t)^3$ times the initial skewness, which is zero for gaussian initial conditions. Similarly, at linear order, all higher order moments will be proportional the initial ones; thus a normal PDF remains normal in linear theory. The second order solution (7) shows that the second term involves $\langle \varepsilon^4 \rangle$, which is $\propto \sigma^4$ for gaussian initial conditions. Thus the skewness ratio

$$S_3 \equiv \frac{\langle \delta^3 \rangle}{\langle \delta^2 \rangle^2} \quad (11)$$

is a constant versus scale, and one finds (ref. [8]) up to terms of order ε^2 (since $\langle \varepsilon^5 \rangle = 0$),

$$S_3 = 4 + 4\kappa(\Omega) \simeq \frac{34}{7} + \frac{6}{7}(\Omega^{-2/63} - 1). \quad (12)$$

The \simeq sign above applies to the range of applicability of equation (9). The first term of this equation, $34/7$, had been obtained by Peebles more than a decade ago (LSS, §18).

The weak Ω -dependence of the full expression shows that nearly all the Ω -dependence of the skewness $\langle \delta^3 \rangle$ comes from that of the square of the variance. It simply reflects the fact that the second order growth rate is nearly equal to $D(t)^2$, as can be seen from (7).

3.2.2. Smoothing the density field: to make contact with observables, we want the skewness of the density field δ_ℓ , when *smoothed* with either a top-hat or a gaussian (spherically symmetric) window, which satisfies

$$\int W(x) d^3x = 1, \quad \text{and} \quad \int W(x) x^2 d^3x = \ell^2 .$$

The first equation insures a proper normalization to unity, while the second requires the effective half-width ℓ to be finite. The top hat case is appropriate for comparisons with the observed frequency distribution of galaxies. (In that case, discreteness corrections must be taken into account before comparing with the theory, *e.g.*, $\langle (N/\bar{N} - 1)^2 \rangle = 1/\bar{N} + \langle \delta^2 \rangle$ if one adopts the Poisson model, see *e.g.*, LSS §33. A gaussian window, on the other hand, removes these discreteness fluctuations, since it does not have sharp edges.) Here we recall the main results of [31].

The calculations are most conveniently done in Fourier space. For the initial field ε , the Fourier components are given by

$$\varepsilon_{\mathbf{k}} \equiv \frac{1}{(2\pi)^{3/2}} \int \varepsilon(\mathbf{x}) \exp(i\mathbf{k} \cdot \mathbf{x}) d^3x .$$

For gaussian initial conditions, one has

$$\begin{aligned} \langle \varepsilon_{\mathbf{k}} \varepsilon_{\mathbf{k}'} \rangle &= \delta_D(\mathbf{k} + \mathbf{k}') P(k), & \langle \varepsilon_{\mathbf{k}} \varepsilon_{\mathbf{k}'} \varepsilon_{\mathbf{q}} \rangle &= 0, \\ \langle \varepsilon_{\mathbf{k}} \varepsilon_{\mathbf{k}'} \varepsilon_{\mathbf{q}} \varepsilon_{\mathbf{q}'} \rangle &= P(k) P(q) \delta_D(\mathbf{q} + \mathbf{q}') \delta_D(\mathbf{k} + \mathbf{k}') + \text{cycl. (2 terms)}, \end{aligned} \quad (13)$$

where δ_D is the Dirac delta, and $P(k)$ is the (initial) power spectrum. Now we can use (10) and (7) to derive S_3 to lowest non-vanishing order,

$$S_3 = \int \frac{d^3k d^3k'}{(2\pi)^6 \sigma^4} P(k) P(k') W_{\mathbf{k}} W_{\mathbf{k}'} W_{|\mathbf{k}-\mathbf{k}'|} T(\mathbf{k}, \mathbf{k}') + O(\sigma^2) . \quad (14)$$

Here $T(\mathbf{k}, \mathbf{k}')$ stands for $T(\mathbf{k}, \mathbf{k}') = 4 + 4\kappa(\Omega) - 6\mu(k/k') + [2 - 4\kappa(\Omega)] P_2(\mu)$, where $\mu = \mathbf{k} \cdot \mathbf{k}' / kk'$, and P_2 is a Legendre polynomial. If there is no smoothing ($W_{\mathbf{k}} = 1$), the dipole and quadrupole terms integrate to zero, and one simply recovers (12). On the other hand, as soon as one introduces smoothing, the result *does depend on the initial power spectrum* $P(k)$.

Let us assume that $P(k) \propto k^n$. Then, for a top-hat smoothing, and $-3 \leq n < 1$, the equation (14) yields after painful calculations the simple result

$$S_3 = 4 + 4\kappa(\Omega) - (3 + n) . \quad (15)$$

Actually, a careful inspection of the expression (14) shows that S_3 should only depend on the effective (logarithmic) slope of the power spectrum at the smoothing scale. This was confirmed in [31] (see also figure 1) by comparing numerical integration for a CDM power spectrum with a prediction using (15). The result above was generalized in [4] to an arbitrary gaussian field, smoothed with a top hat filter on a scale ℓ ,

$$S_3(\ell) = 4 + 4\kappa(\Omega) - \gamma_\ell, \quad \text{with} \quad \gamma_\ell = -\frac{\partial \log \langle \delta^2 \rangle}{\partial \log \ell} .$$

For a pure power law $P(k)$, we have $\gamma = 3 + n$, in agreement with (15).

The rather messy calculations involved in computing the case of smoothing by a gaussian were recently completed in [36] who express it in terms of hypergeometric functions:

$$S_3 = 3 {}_2F_1\left(m, m, \frac{3}{2}, \frac{1}{4}\right) - \left(n + \frac{8}{7}\right) {}_2F_1\left(m, m, \frac{5}{2}, \frac{1}{4}\right) \quad (16)$$

with $m = \frac{n+3}{2}$. The behavior of this expression with the spectral indices n and Ω is in fact very similar to that of the top-hat case, see figure 7.2 below.

3.2.3. Skewness of the Velocity Field PDF The continuity equation gives the divergence of the velocity field in terms of the time derivative of the density contrast. Let us call T_3 the skewness ratio for the divergence of the velocity field in units of the Hubble constant ($\theta = \nabla \cdot \mathbf{v}/H$). One then finds [6] for a top-hat smoothing,

$$T_3 \equiv \frac{\langle \theta^3 \rangle}{\langle \theta^2 \rangle^2} = -\Omega^{-0.6} \left[\frac{26}{7} - \gamma_\ell \right]. \quad (17)$$

The corresponding (complicated) expression for the a gaussian window has recently been obtained (together with the corresponding S_3) in [36].

The asymmetry in the distribution of θ is directly related to the asymmetry in δ : voids and clusters in the mass distribution correspond to sources ($\theta > 0$) and sinks ($\theta < 0$) in the velocity field. This quantity has the same dependence in Ω than the ratio of the predicted versus observed velocity in density-velocity field comparisons, but it uses an intrinsic property of the field, thereby bypassing reference to the density field and to an unknown biasing parameter.

It turns out that θ may be advantageously measured by using Voronoi or Delaunay tessellations of space [7]. It remains to be seen whether these methods provide accurate and unbiased estimators of T_3 when the number of sampling points is comparable to those of observed catalogs, and one has only the line-of-sight velocity (*i.e.*, bypassing the use of a POTENT-like machinery). First analyses [28] are encouraging in that regard. Finally, let us note that an analytical expression for T_3 in the gaussian smoothing case has recently been obtained (together with the corresponding S_3) in [36].

3.2.4. Kurtosis Using similar techniques to those described above, one can compute the Kurtosis coefficient

$$S_4 = \frac{\langle \delta^4 \rangle - 3\sigma^4}{\sigma^6}$$

and the corresponding T_4 for the expansion scalar θ . One finds [4] for a top hat smoothing

$$S_4 = \frac{60712}{1323} - \frac{62}{3}\gamma_\ell + \frac{7}{3}\gamma_\ell^2, \quad T_4 = \frac{1}{f(\Omega)} \left[\frac{12088}{441} - \frac{338}{21}\gamma_\ell + \frac{7}{3}\gamma_\ell^2 \right].$$

This was actually derived an equation for the evolution of the full generating function (see below). The corresponding expressions for a Gaussian smoothing can be found in [36].

3.3. Edgeworth Expansion of the PDF

As was shown in [32], the previous results on the moments of the PDF in the weakly non-linear regime can be used to examine how gravitational instability drives a PDF away from its initial state. Let us start with the density field PDF, $P(\delta, \ell)$, or rather $p(\nu)$, the PDF of the density field in terms of the standardized random variable $\nu \equiv \delta_\ell / \sigma_\ell$. Since we want to describe an evolution from gaussian initial conditions, it makes sense to consider an expansion of $p(\nu)$ in terms of $\phi(\nu) = (2\pi)^{-1/2} \exp(-\nu^2/2)$ and its derivatives. The *Gram-Charlier series* (Cramér 1946 and references therein) provides such an expansion:

$$p(\nu) = c_0 \phi(\nu) + \frac{c_1}{1!} \phi^{(1)}(\nu) + \frac{c_2}{2!} \phi^{(2)}(\nu) + \dots, \quad (18)$$

where c_m are constant coefficients. Superscripts denote derivatives with respect to ν :

$$\phi^{(m)}(\nu) \equiv \frac{d^m \phi}{d\nu^m} = (-1)^m H_m(\nu) \phi(\nu), \quad (19)$$

where H_m is the Hermite polynomial of degree m . The Hermite polynomials satisfy orthogonality relations (e.g. Abramowitz & Stegun 1964), $\int_{-\infty}^{\infty} H_m(\nu) H_p(\nu) \phi(\nu) d\nu = 0$, if $m \neq p$, and $= m!$ otherwise. Therefore, multiplying both sides of equation (18) by H_m and integrating term by term yields

$$c_m = (-1)^m \int_{-\infty}^{\infty} H_m(\nu) p(\nu) d\nu. \quad (20)$$

Equation (20) gives $c_0 = 1$, $c_1 = c_2 = 0$, while for the next four coefficients in the series we obtain

$$c_m = (-1)^m S_m \sigma_\ell^{m-2}, \quad \text{for } 3 \leq m \leq 5; \quad c_6 = S_6 \sigma_\ell^4 + 10 S_3^2 \sigma_\ell^2. \quad (21)$$

Thus the $S_m(\ell)$ have both a dynamic and a static application: they describe the time evolution of moments of the PDF at a fixed smoothing scale ℓ , and they also describe the relation between moments of the PDF at a fixed time on different smoothing scales. In the latter case, one must also include the scale-dependence of the S_m if the initial power spectrum is not scale-free.

We have seen that perturbation theory and gaussian initial conditions imply that $\langle \delta_\ell^3 \rangle \propto \sigma_\ell^4$, and S_3 is therefore an ‘‘order unity’’ quantity when σ_ℓ is the ‘‘small’’ parameter. The same is true for all remaining reduced moments, $S_m = O(1)$ for all m [3] & [22]. It implies that the Gram-Charlier series *is not* a proper asymptotic expansion for $p(\nu)$. In an asymptotic expansion, the remainder term should be of higher order than the last term retained. However, if we truncated the series (18) at the $\phi^{(4)}$ term, which is $O(\sigma^2)$, we would miss another $O(\sigma^2)$ contribution coming from c_6 (equation (21)). In order to deal with this problem, let us rearrange the Gram-Charlier expansion by collecting all terms with the same powers of σ . The result is the so-called *Edgeworth series*, with the first terms given by

$$p(\nu) = \phi(\nu) - \frac{\sigma}{3!} S_3 \phi^{(3)}(\nu) + \left[\frac{1}{4!} S_4 \phi^{(4)}(\nu) + \frac{10}{6!} S_3^2 \phi^{(6)}(\nu) \right] \sigma^2 + O(\sigma^3). \quad (22)$$

Cramér [17]) lists the Edgeworth series to higher order, and he proves that it is a proper asymptotic expansion. This proof is directly relevant to our purposes, since it implies that there are no additional $O(\sigma^2)$ terms hiding in the Gram-Charlier series at

$m > 6$. The Edgeworth series thus provides a series expansion for the evolving PDF in powers of the r.m.s. fluctuation σ .

Of course, if the variable we are interested in is θ instead of δ , one just adopts the appropriate analogues of S_m , *e.g.*, $S_3 \rightarrow T_3 \equiv \langle \theta^3 \rangle \langle \theta^2 \rangle^{-2}$, and so on. Similarly, if we are interested in the PDF shape in redshift space, one just needs to use the corresponding analogue of S_m , S_m^z , see §7.2). The Edgeworth series may also be used to relate S_3 to other measures of asymmetry like $\langle \delta|\delta| \rangle$ which, according to [41] may offer better signal to noise ratio than $\langle \delta^3 \rangle$ when applied to real galaxy surveys (by being less sensitive to the tail of the PDF, *i.e.*, to rare events). This latter quantity is not easy to compute directly by perturbation theory (see the appendix of [32]), but it is trivial to obtain

$$\langle \delta|\delta| \rangle = \sqrt{\frac{2}{9\pi}} S_3 \sigma^3 + O(\sigma^5). \quad (23)$$

by using the Edgeworth series.

3.4. Validity of Perturbation Theory

The previous results assume that the system never gets to be strongly non-linear, *i.e.*, $\sigma_\ell \ll 1$ is true at *every* scale. But in the real universe, we know that the observed density contrast is very large at small scales. One only gets $\sigma_\ell \ll 1$ for $\ell \gg 8h^{-1}$ Mpc. It is thus by no means obvious that there is any range today for which perturbation theory might be applicable. On the other hand, it has long ago been noticed that linear perturbation theory yields a good description of the variance [or the 2-body correlation function $\xi(t) \propto D(t)^2/D(t_i) \xi(t_i)$] measured in fully non-linear numerical simulation.

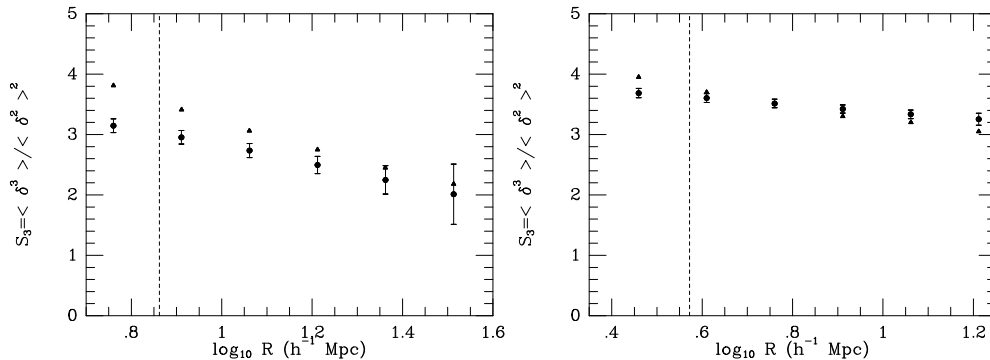


Figure 1. The measured $S_3(\ell)$ in a CDM simulation (triangles) is compared to the theory (circles; the error bars come from the numerical uncertainty in evaluating the integrals giving S_3). The left panel corresponds to a spherical top-hat smoothing, while the right one corresponds to a gaussian smoothing. The vertical dashes mark the limit between the strongly non-linear regime ($\sigma \geq 1$) and the weakly non-linear one ($\sigma \leq 1$). Courtesy Colombi 1993 & Juszkiewicz *et al* 1993a.

It turns out that what holds true for linear perturbation theory results is also true at higher orders. Indeed, the top-hat expressions for S_3 have been checked against the simulation results in [19], [9] & [34], in the case of scale-free initial spectra. In the case of a gaussian smoothing, the theory was checked with the scale free-simulations

in [48]. In the CDM case, comparison were made with the results in [9], as well as simulations performed for that purpose, see figure 1. In all those cases, the agreement between the perturbation theory and N-body experiments was excellent (see [31] for further details), up to surprisingly large values of the variance ~ 1 .

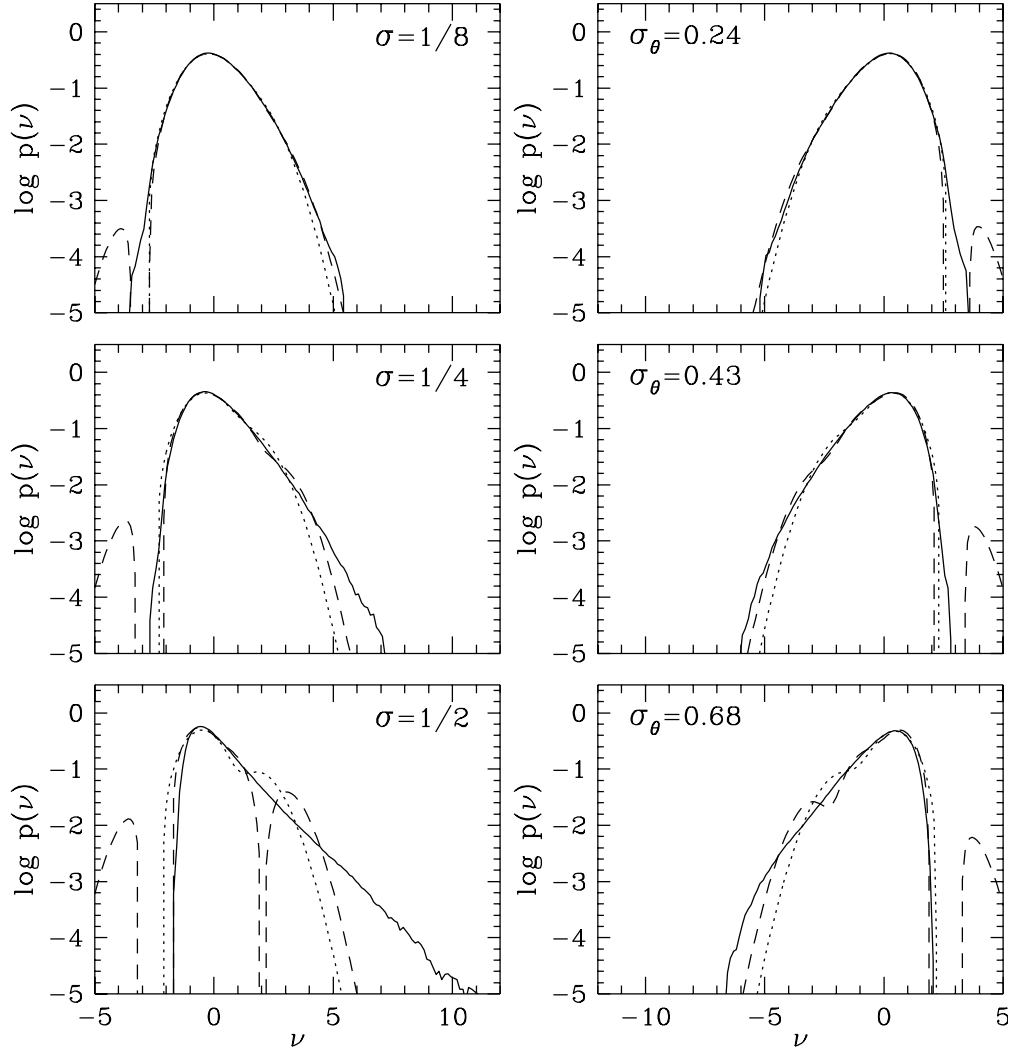


Figure 2. Comparisons of the Edgeworth PDF with simulations (solid lines). See details in the text. Courtesy Juszkiewicz *et al* 1993b.

One can also check when the Edgeworth series and perturbation theory are appropriate to describe the overall shape of the PDF. The solid lines of figure 2 show the PDF of the smoothed density fields of matter density (left column) and velocity divergence (right column), at three different stages in scale-free $n=-1$ simulations. The corresponding rms amplitude (σ and σ_θ) are shown in each panel, and the variables on the horizontal axes are $\nu = \delta/\sigma$ and $\nu = \theta/\sigma_\theta$. In all the panels, dotted and dashed lines show the approximations keeping the terms of order σ and σ^2 respectively in

eq. (22). The approximations work well for $S_3\sigma < 1$ and $|\nu\sigma| < 1$ (and equivalent requirements for θ). They begin to break down outside of that range, as expected.

So far, all the comparisons done lead to the same conclusion: perturbation theory predicts remarkably accurately the simulation results when $\sigma \lesssim 1$ ($|\nu\sigma| < 1$ for the Edgeworth PDF), even when small scales are strongly non-linear. All the discrepancies found could actually be traced to limitations of the simulations themselves. What remains to be found though, is why perturbation works so well, even at scales where the density contrast is comparable to unity.

4. FURTHER DEVELOPMENTS

4.1. Higher Order Moments

While appropriate to break fresh grounds, the pedestrian calculation approach used so far would be quite unwieldy to compute higher order moments. Fortunately, Bernardeau [3] found an elegant shortcut by means of a dynamical equation for the generating function of quantities closely related to the moments. This function simply obeys the evolution equation of the spherical collapse. One nice aspect of this approach is that it also gives the moments hierarchy for approximate descriptions of the dynamics (like those described in § 7.3 and afterwards). Indeed, in that case, the moments are then obtained from the generating function obeying the evolution equation of the spherical collapse, as given by the considered approximation [40]. In addition, this approach was successfully generalized to account for a top-hat smoothing [4]. Unfortunately, this generalization uses a trick specific to the top-hat case. Gaussian smoothing calculation still have to be done “by hand”. used for

4.2. Higher Order Corrections to the Moments

All the calculations presented so far were performed retaining only the leading non-linear corrections, that is in the limit $\sigma \rightarrow 0$. Recently, though, the next higher order correction to all moments was obtained [46], albeit in the absence of smoothing. These (one-loop) corrections start to dominate the leading non-linear (tree-level) corrections when $\sigma \sim 1/2$ for the density field and $\sigma \sim 1$ for the divergence of the velocity field.

The only case so far when these one-loop correction were obtained in the presence of smoothing is for the simplest moment, the variance itself [37]. One can then approach the long-standing “previrialisation” problem: do the presence of small scale slows down the collapse of larger structures encompassing them? Or in other words, do non-linear interactions between different scales increase or decrease the rate of growth of structures. Perturbation theory can at least give us a hint of what the first non-linear corrections do. Lokas *et al* [37] find that the weakly non linear growth of variance is very similar to the linear one, when the index n of the primordial power spectrum is close to -1, in agreement with the numerical simulation results of [20] who concluded to the absence of a previrialisation effect. But it is decreased if it is shallower, i.e. if small scale structures are more prominent. This does bring support to Peebles’ (very educated) guess when he argued that small scale structures will promote the development of non-radial motions in the larger collapsing region, these motions acting effectively as a stabilizing pressure term. Once again, those perturbative results are confirmed by simulations results, as can be seen on figure 3.

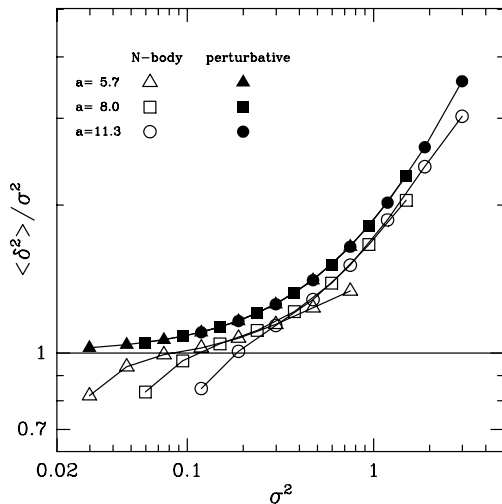


Figure 3. Previrialisation effect in the $n = -2$ case. Courtesy Lokas *et al* 1995b.

4.3. General Initial Conditions

So far, we focused our attention to the case of Gaussian initial conditions for which the reduced moments, or cumulants, are initially zero, and thus S_3 and S_4 too. We found that in this specific case, the S_3 and S_4 which develop under the influence of gravity take on particular *constant* values. But what happens for more generic initial conditions? Can the predictions for the Gaussian case can be used as observational tests of the Gaussian hypothesis?

Initially, one expects on dimensional grounds to have $\langle \delta^3 \rangle \propto \sigma^3$, i.e. $S_3 \propto 1/\sigma$. But non-gaussian fluctuations will also built a gravitationally induced contribution during their evolution, which may quickly dominate the initial term. This was demonstrated in specific cases by [15] & [38], and [24] succeeded in performing the calculation for arbitrary initial conditions. They found that $s = \langle \delta^3 \rangle / \sigma^3$ is equal to its initial value, s_i plus a term proportional to σ , the coefficient of proportionality depending on the assumed initial conditions. Unfortunately, biasing (see below) may change this proportionality constant, thus comparisons to data will only put an upper limit on s_i .

Fortunately, as shown in [14], similar calculation at the next order show that $k = \langle \delta^4 \rangle / \sigma^4$ is equal to its initial value k_i plus a term linear in σ . This term is zero in the gaussian case (the first non-zero term is in σ^2 , leading to a constant S_4). This measure should thus be a more powerful probe of the gaussian hypothesis, since then this is the scaling with σ which is altered in the generic case, not a coefficient in front. The gravitational evolution is then less likely to cast a shadow on the signature of non-gaussian initial conditions.

4.4. Biasing and comparisons to data

As was mentioned earlier, it might be that galaxies are not fair tracers of the mass, even at the large scales where perturbation theory is applicable. But let us suppose that this biasing is local, *i.e.*, that the galaxy field at scale ℓ , $\delta_{g,\ell}$ is some unknown function B of the underlying field at the same location, $\delta_{g,\ell}(x) = B[\delta_\ell(x)]$. Then a

Taylor expansion would give

$$\delta_g = \sum_{k=0} \frac{b_k}{k!} \delta^k,$$

where b_0 is set so that $\langle \delta_g \rangle = 0$, b_1 is the *linear* bias introduced previously, and $b_k = d^k B / dy^k |_{y=0}$. Replacing this into the expression for skewness, one sees that the galactic field skewness, S_3^g , is given by [32]

$$S_3^g = \frac{S_3}{b_1} + \frac{3b_2}{b_1^2}. \quad (24)$$

If the biasing is not scale-dependent (why should it be on very large scales?), then the constancy with scale of S_3 is preserved. This agrees well with the determination [11] in the *IRAS* 1.2Jy catalog (see fig. 4) or in the SSRS [26]. In addition, if a linear bias is assumed, like it is customary in density-velocity comparisons for measuring $\beta = \Omega^{0.6}/b_1$, then one gets the linear bias parameter b_1 , *independently* of the (poorly known!) value of Ω . Indeed, once the shape of the window function is fixed, S_3 depends in a known way on the local slope of the power spectrum only, which can be determined self-consistently by measuring the slope of the second moment in the same catalog.

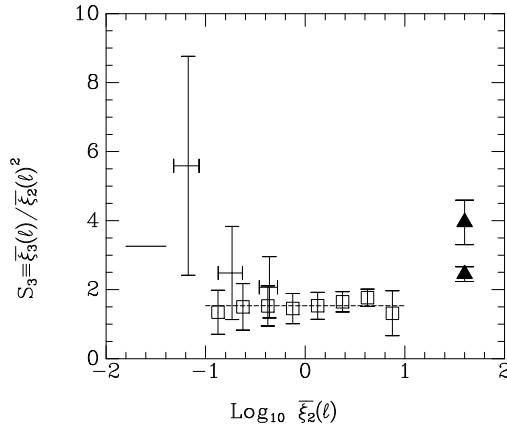


Figure 4. Skewness measurement in the *IRAS* 1.2 Jy catalog. Courtesy Bouchet *et al* 1993)

Of course, there might be a non-linear biasing term, b_2 , and a skewness measurement alone will then only constrain the combination (24). One cannot hope to break this degeneracy by measuring the galactic field kurtosis, since then a new unknown, b_3 , would enter the game. On the other hand, one can compare measurements in different catalogs, e.g. optically and infrared selected, to obtain ratios of biasing parameters [23] (see also [35]). In addition, by extending systematically considerations similar to those above, [23] develop a general (local) bias transformation theory and show that the signature of gaussian initial conditions evolving under gravity, i.e. $S_n = \text{constant}$ is preserved by a local biasing, i.e. S_n^g remains a constant (with a different value) at all orders n . On the contrary, as was shown in [21], a cooperative galaxy formation scheme can be severely constrained by the skewness it would predict.

Finally, let us mention that a similar scaling of the moments with the second one has been found in the APM survey [25], which is indeed expected [5] theoretically.

5. ZELDOVICH APPROXIMATION

As was shown above, a lot can be accomplished by using the standard Eulerian perturbative approach to gravitational instability. However, perturbative equations are often easier to integrate when expressed in Lagrangian coordinates. In our experience, this happened at second order for $\Omega \neq 1$ (see §6.1 below). Another example is the redshift space distortion for $\langle \delta^3 \rangle$, discussed in §7.2. Moreover, as $\langle \delta^2 \rangle$ grows with time, at any fixed order in perturbation theory, the Lagrangian approach is likely to remain valid longer than the Eulerian approach. This is so because the requirement of small Lagrangian displacements and gradients is weaker than the requirement $\langle \delta^2 \rangle \ll 1$. This idea, which motivated Zel'dovich [49] approximation (which is simply the extrapolation of the first order Lagrangian solution in a regime where its validity is not mathematically warranted), remains valid at higher orders.

In the following, I first introduce Zel'dovich approximation by using previous results concerning the linear Eulerian theory. I then discuss an application to the growth of galactic spin (tidal torque theory), as well as the idea of ‘‘Pancakes’’.

In a second step, I outline the general derivation of the perturbative (Lagrangian) solutions, and focus on the redshift distortion problem as an application. I also give examples of comparison between Eulerian and Lagrangian theory when $\langle \delta^2 \rangle \simeq 1$, i.e. when Zel'dovich and higher order approximations are used as approximations to the real dynamics, in a regime where their validity is hard to assess analytically.

5.1. Derivation from Eulerian Theory

We found above that in linear Eulerian theory the evolution of the growing mode is self-similar, with

$$\delta(\mathbf{x}, \tau) = D(\tau)\varepsilon(\mathbf{x}), \quad \phi(\mathbf{x}, \tau) = \frac{D}{a}\phi_i(\mathbf{x}); \quad \nabla^2\phi_i = 4\pi G\rho_b a^3\varepsilon(\mathbf{x}),$$

the subscript i referring to an ‘‘initial’’ state. Note that in an Einstein–de Sitter Universe, $D(\tau) \propto a$, and thus the potential is (linearly) conserved. In addition, the linearized Euler equation using the conformal time τ , $a\dot{\mathbf{v}} + \dot{a}\mathbf{v} = -a\nabla\phi = -D\nabla\phi_i$ (with $\mathbf{v} = \dot{\mathbf{x}}$) yields $\mathbf{v} = -(1/a)\int Dd\tau\nabla\phi_i = -(1/D)\int Dd\tau\nabla\phi$ (i.e. \mathbf{v} is parallel to $\nabla\phi$).

We can thus use these expressions to get the linear trajectory of a particle as a displacement field, $\Psi(t, \mathbf{q}) = \mathbf{x} - \mathbf{q}$, applied to its initial position, or Lagrangian coordinate, \mathbf{q} ,

$$\mathbf{x} = \mathbf{q} + \Psi(\tau, \mathbf{q}) \quad \text{with} \quad \Psi = \left[\int \frac{d\tau}{a} \int Dd\tau \right] \nabla\phi_i. \quad (25)$$

By using the continuity equation written as $a\ddot{D} = \dot{a}D = 4\pi G\rho_b a^3 D$, we obtain

$$\Psi(\tau, \mathbf{q}) = b(\tau)\Psi_i, \quad \text{with} \quad b(\tau) = \frac{D(\tau)}{4\pi G\rho_b a^3}, \quad \Psi_i = \nabla\phi_i, \quad (26)$$

the velocity field being given by $\mathbf{v} = -a\dot{b}\Psi_i$. At the linear order then, particles just go straight (in comoving coordinates) in the direction set by their initial velocity.

Zeldovich' approximation is to use these linear solutions to extrapolate fluid element trajectories well beyond the validity range of the linear Eulerian theory ($\delta \ll 1$).

5.2. Galactic Spin Origin

Zeldovich approximation allows to see quite easily how the tidal field of an inhomogeneous distribution couples to the quadrupole of the mass distribution of a proto-object to induce a growth of its angular momentum \mathbf{M} . At early times,

$$\mathbf{M} = \int_V d^3q \rho a^3 (a\mathbf{x} - a\bar{\mathbf{x}}) \wedge \mathbf{v}/a,$$

where the integral is taken over the initial (lagrangian) volume of the perturbation V , of center of mass $\bar{\mathbf{x}} = \int_V d^3q \mathbf{x}/V$. At the lowest order, $\rho \equiv \rho_b$ and $\mathbf{v} = -a\dot{b}\nabla\phi_i$, and thus

$$\mathbf{M} = -\rho_b a^4 \dot{b} \int_V d^3q (\mathbf{q} - \bar{\mathbf{q}}) \wedge \nabla\phi_i = -\rho_b a^4 \dot{b} \int_S \phi_i (\mathbf{q} - \bar{\mathbf{q}}) \wedge dS.$$

The second expression follows by integration par part (Gauss' divergence theorem), and the integral is thus taken over the boundary surface of the lagrangian volume of the future object. If this volume is spherical (or its surface S is an equipotential), then \mathbf{M} remains zero. Provided the initial potential is smooth enough, we can take advantage of a Taylor expansion of the acceleration around the center of mass,

$$\nabla\phi_i|_{\mathbf{q}} = \nabla\phi_i|_{\bar{\mathbf{q}}} + (\mathbf{q} - \bar{\mathbf{q}}) \cdot \nabla\nabla\phi_i|_{\bar{\mathbf{q}}} + \mathcal{O}[(\mathbf{q} - \bar{\mathbf{q}})^2],$$

to relate the angular momentum to the inertia tensor of the proto-object, \mathcal{I} , and the (initial) tide tensor at the center of mass position, \mathcal{T} defined in (8),

$$M_i = -a\dot{b}\epsilon_{ijk}T_{jl}I_{lk}, \quad \text{with} \quad \mathcal{I}_{lk} = \int_V (q_l - \bar{q}_l)(q_k - \bar{q}_k)\rho_b a^3 d^3q,$$

ϵ standing for the totally antisymmetric tensor of order 3.

In the Einstein-de Sitter case, the linear growth rate of the angular momentum is thus

$$\mathbf{M} \propto \tau^3 \propto t.$$

Of course, this description holds only during the early collapse phase (\sim while the proto-object is still expanding). Later one, particle turn over, and there is no chance that their trajectories may be described by a simple ballistic approximation. Latter phases have been mostly studied by numerical simulations. Still, the simple exercise above shows how Zeldovich approximation clearly unveils the basic principle of the tidal torque theory of the galactic spin origin, i.e. that the tidal field of neighboring density perturbation acts on the irregular shape of the proto-object.

5.3. Density Contrast & Pancakes

The density contrast simply obtains from the trajectories by requiring that mass be conserved, i.e.

$$\rho(\tau)d^3x = \rho(\tau_i)d^3q \implies 1 + \delta = \frac{1}{J},$$

J standing for the Jacobian of the transformation from \mathbf{q} to \mathbf{x} :

$$J = \left| \frac{\partial \mathbf{x}}{\partial \mathbf{q}} \right| = |\det \mathcal{D}|.$$

The deformation tensor, \mathcal{D} may be written as the identity matrix plus the tidal tensor $T = |\partial \Psi / \partial \mathbf{q}|$, which is directly given by the curvature of the initial potential field (in Zeldovich approximation, $T = b \nabla \nabla \phi_i / (4\pi G \rho_b a^3)$).

Let us call $\lambda_1 \geq \lambda_2 \geq \lambda_3$ the local eigenvalues of the (initial) tidal field. The density contrast may then be written as

$$1 + \delta = \frac{1}{[1 - b(\tau)\lambda_1][1 - b(\tau)\lambda_2][1 - b(\tau)\lambda_3]},$$

which shows that, if this approximation remains approximately valid till the first crossing of trajectories, one expect a singularity, a (locally) planar collapse to infinite density along the axis of the largest positive (if any) eigenvalue, λ_1 , when $b(\tau)\lambda_1 \rightarrow 1$. If no eigenvalue is positive, this is a developing underdense region, while in the rarer case when two eigenvalues are approximately equal, $\lambda_1 = \lambda_2 \neq \lambda_3$, there is a collapse to a filament. The case $\lambda_1 = \lambda_2 = \lambda_3$ leads to a spherical collapse.

For a gaussian field, Doroshkevich found the probability distribution of the eigenvalues, and in particular that $P(\lambda_1 > 0, \lambda_2 < 0, \lambda_3 < 0) = 0.42$ ($= P(\lambda_1 < 0, \lambda_2 > 0, \lambda_3 > 0)$). It shows that indeed one generically expects “pancakes” around local maxima of λ_1 . This is to be contrasted with the *linear* Eulerian theory whose extrapolation would lead to predicting a collapse around the initial maxima of the density field (since $\delta \propto \delta_i$), i.e. around local maxima of $\lambda_1 + \lambda_2 + \lambda_3$ whose collapse is rather spherical.

The “pancake” theory arose in the context of a “neutrino” dominated dark matter, where there is a natural small scale cut-off in the power spectrum of perturbations due to their early phase of free-streaming. Then the potential field is quite smooth and it is not too surprising that Zeldovich approximation provides a quite accurate description of the large scale structures which appear in numerical simulations. Indeed, we only have to describe an essentially laminar flow. On the other hand, in a hierarchical scenario where small scale structures collapse first, these small scale potential wells will undoubtedly curve the particles trajectories and Zeldovich approximation would not describe at all the individual particle trajectories. We shall see later that this approximation might still be useful, but in an average sense.

6. LAGRANGIAN PERTURBATION THEORY

In the previous section, we made contact with a lagrangian description of the dynamics by introducing Zeldovich approximation as a consequence of the Eulerian perturbation theory at the linear order. In the following, we rather describe the steps involved in a systematic perturbative approach of Lagrangian theory, as initiated by Moutarde *et al* 1991, [39] (see also the contribution of T. Buchert in this volume). We then proceed with an application to these results to the computing of the skewness in redshift space. We shall later come back to using those rigorous perturbative solution as approximations to the full non-linear dynamics, thereby extending Zeldovich ansatz.

6.1. Perturbative equations

The Lagrangian perturbative approach introduced by Moutarde *et al* (1991) proceeds in quite a parallel fashion to the Eulerian one reviewed earlier. As before, we use the Newtonian approximation with comoving coordinates (see the contribution of S. Matarese in this volume for the full general relativistic approach). Following Doroshkevich *et al* 1973 [18], we replace the standard cosmological time by a new time τ defined by

$$d\tau \propto a^{-2} dt. \quad (27)$$

Beware that we kept the same symbol here than above for the conformal time (which is defined instead by $ad\tau \propto dt!$). In that case the motion and field equations now read

$$\ddot{\mathbf{x}} = -\nabla_x \Phi, \quad \Delta_x \Phi = \beta(\tau)\delta, \quad (28)$$

with no $\dot{\mathbf{x}}$ term. In this equation, dots denote derivatives with respect to τ , and $\beta(\tau) = 4\pi G a(\bar{\rho} a^3)$. By choosing properly the proportionality constant in the definition (27) when, respectively, Ω is equal, smaller or greater than 1, β is simply given by

$$\beta = \frac{6}{\tau^2 + k(\Omega)},$$

with $k(\Omega = 1) = 0$, $k(\Omega < 1) = -1$, and $k(\Omega > 1) = +1$. While $\tau = t^{-1/3}$, when $\Omega = 1$, one has $\tau = |1 - \Omega|^{-1/2}$ otherwise.

Now we wish to follow the particle trajectories instead of the density contrast, by using the mapping

$$\mathbf{x}(\tau) = \mathbf{q} + \Psi(\tau, \mathbf{q}) \quad (29)$$

The Jacobian of the transformation from \mathbf{x} to \mathbf{q} , permits as before to express the requirement of mass conservation simply as

$$\rho(\mathbf{x}) J d^3 q = \rho(\mathbf{q}) d^3 q,$$

i.e., $\delta = J^{-1} - 1$ (note that $\rho(\mathbf{x})$ is in fact a shorthand for $\rho(\mathbf{q}, t)$). By taking the divergence of the equation of motion (28), one obtains the equivalent of the Eulerian equation (4):

$$J(\tau, \mathbf{q}) \nabla_x \ddot{\mathbf{x}} = \beta(\tau) [J(\tau, \mathbf{q}) - 1]. \quad (30)$$

Of course the addition of any divergence-free displacement field to a solution of the previous equation will also be a solution. In the following, we remove this indeterminacy by restricting our attention to potential movements, which must satisfy

$$\nabla_x \times \dot{\mathbf{x}} = 0. \quad (31)$$

The main reason to restrict to that case is that vortical perturbations linearly decay, a consequence of the conservation of angular momentum in an expanding universe. Thus one might consider that the solutions will apply anyway, even if vorticity is initially present, because at later times it will decay away. In the same spirit, we shall mainly focus on growing mode solution (see [12, 13] for the cases of rotational perturbations in Lagrangian space but not in Eulerian space, and also for the effect of decaying modes).

The final equation to solve obtains by rewriting the divergence of the acceleration $\Gamma \equiv \ddot{\mathbf{x}}$ explicitly as a function of \mathbf{q}

$$\nabla_x \Gamma = J(\tau, \mathbf{q})^{-1} \sum_{i,j} \Gamma_{i,j} A_{ji}, \quad (32)$$

where the A_{ij} are the cofactors of the Jacobian, and the partial derivatives denoted by Latin letter are taken with respect to the \mathbf{q} coordinate (e.g., $\Gamma_{i,j} = \frac{\partial \Gamma_i}{\partial q_j}$).

As in the Eulerian case, perturbative solutions are obtained by means of an iterative procedure. But this time, the expansion concerns the particles displacement field itself, and we write it as

$$\Psi = \varepsilon \Psi^{(1)} + \varepsilon^2 \Psi^{(2)} + \varepsilon^3 \Psi^{(3)} + \mathcal{O}(\varepsilon^4). \quad (33)$$

The determinant of the Jacobian is then similarly expanded as

$$\begin{aligned} J &= 1 + \varepsilon J^{(1)} + \varepsilon^2 J^{(2)} + \varepsilon^3 J^{(3)} + \mathcal{O}(\varepsilon^4) \\ &= 1 + \varepsilon K^{(1)} + \varepsilon^2 (K^{(2)} + L^{(2)}) \\ &\quad + \varepsilon^3 (K^{(3)} + L^{(3)} + M^{(3)}) + \mathcal{O}(\varepsilon^4) \end{aligned} \quad (34)$$

where $K^{(m)}$, $L^{(m)}$, and $M^{(m)}$ denote the m -th order part of the (invariant) scalars

$$\begin{cases} K &= \nabla \cdot \Psi = \sum_i \Psi_{i,i} \\ L &= \frac{1}{2} \sum_{i \neq j} (\Psi_{i,i} \Psi_{j,j} - \Psi_{i,j} \Psi_{j,i}) \\ M &= \mathcal{D} = \det[\Psi_{i,j}]. \end{cases}$$

In other words,

$$\begin{cases} K^{(m)} &= \nabla \cdot \Psi^{(m)} = \sum_i \Psi_{i,i}^{(m)} \\ L^{(2)} &= \frac{1}{2} \sum_{i \neq j} (\Psi_{i,i}^{(1)} \Psi_{j,j}^{(1)} - \Psi_{i,j}^{(1)} \Psi_{j,i}^{(1)}) \\ L^{(3)} &= \sum_{i \neq j} (\Psi_{i,i}^{(2)} \Psi_{j,j}^{(1)} - \Psi_{i,j}^{(2)} \Psi_{j,i}^{(1)}) \\ M^{(3)} &= \det[\Psi_{i,j}^{(1)}]. \end{cases} \quad (35)$$

The equation to solve then follows by replacing the expansions (33-35) of the displacement field and of the Jacobian in equations (30) and (32). We now proceed to an iterative solution of this equation.

6.2. Low order Solutions

I give below only the solutions for the first two orders, when $\Lambda = 0$ and Ω is either unity or smaller than one. This is all we need for the application described afterwards. A more complete set in solution can be found in Bouchet *et al* 1995 [10] who give for the first three orders the solutions for arbitrary values of Ω when there is no cosmological constant, as well as numerical solutions for flat universes when $\Lambda \neq 0$.

6.2.1. First Order: keeping only the terms of order ε , one gets

$$\ddot{K}^{(1)} - \beta K^{(1)} = 0. \quad (36)$$

Thus $K^{(1)}(\tau, \mathbf{q})$ can be factorized into a temporal and spatial part, $K^{(1)}(\tau, \mathbf{q}) = g_1(\tau) K^{(1)}(\tau_i, \mathbf{q})$, where $K^{(1)}(\tau_i, \mathbf{q})$ is the divergence of the initial displacement field,

$g_1(\tau_i)$ is assumed to be unity, and $g_1 = k_a g_{1a} + k_b g_{1b}$. For $\Omega = 1$, the linear growth rate g_1 is given by $g_{1a} = \tau^{-2}$, and $g_{1b} = \tau^3$. When $\Omega < 1$,

$$g_{1a} = 1 + 3(\tau^2 - 1)(1 + \tau S), \quad g_{1b} = \tau(\tau^2 - 1), \quad S = \frac{1}{2} \ln \frac{\tau - 1}{\tau + 1}.$$

The closed case is given in [10].

For a potential movement, one thus recovers Zeldovich solution, $\Psi^{(1)}(\tau, \mathbf{q}) = g_1(\tau) \tilde{\Psi}^{(1)}(\mathbf{q})$, as in (25), if we define (for all m)

$$\tilde{\Psi}^{(m)}(\mathbf{q}) \equiv \Psi^{(m)}(\tau_i, \mathbf{q}).$$

Also, note that $\delta^{(1)}(\tau) \propto g_1(\tau)$ (with initially $\delta_i^{(1)} = -\nabla \cdot \tilde{\Psi}^{(1)}(\mathbf{q})$), *i.e.*, the Eulerian linear behavior is recovered, since $g_1 \equiv D$.

The logarithmic derivative of the growth factor, $f_1 \equiv \frac{a}{g_1} \frac{dg_1}{da}$, is useful to describe comoving peculiar velocities and therefore redshift distortions (see below). Near $\Omega = 1$, a limited expansion of the solution shows that $f_1 \asymp \Omega^{4/7}$ where \asymp means ‘‘behaves asymptotically as’’. A better analytical fit for f_1 in the range $0.1 < \Omega < 1$ is given by $f_1 \approx \Omega^{3/5}$, as was originally proposed in [42].

6.2.2. Second Order: collecting terms of $\mathcal{O}(\varepsilon^2)$ in equations (30) and (32), we find

$$\ddot{K}^{(2)} - \beta K^{(2)} = -\beta g_1^2 L^{(2)}(\tau_i, \mathbf{q}). \quad (37)$$

Thus, the solution is again separable, $K^{(2)}(\tau, \mathbf{q}) \equiv g_2(\tau) K^{(2)}(\tau_i, \mathbf{q})$. The spatial part is given by $K^{(2)}(\tau_i, \mathbf{q}) = L^{(2)}(\tau_i, \mathbf{q})$, and the growth factor is

$$g_2 = k_a^2 g_{2a} + 2k_a k_b g_{2b} + k_b^2 g_{2c} + l_a g_{1a} + l_b g_{1b}. \quad (38)$$

For $\Omega = 1$, we simply find $g_{2a} = -\frac{3}{7} g_{1a}^2$, $g_{2b} = \frac{3}{2} g_{1a} g_{1b}$, $g_{2c} = -\frac{1}{4} g_{1b}$, while for $\Omega < 1$,

$$\begin{aligned} g_{2a} &= 1 - \frac{9}{4}(\tau^2 - 1) [\tau + (\tau^2 - 1)S]^2, \\ g_{2b} &= -\frac{3}{4}(\tau^2 - 1) [\tau^3 + (\tau^2 - 1)S], \\ g_{2c} &= -\frac{1}{4}(\tau^2 - 1)^3. \end{aligned} \quad (39)$$

If only a growing mode is initially present ($k_b = 0 = l_b$), which we assume, one must have $g_2/g_1 \rightarrow 0$ when $\tau \rightarrow \infty$, *i.e.*, when $\Omega \rightarrow 1$. A limited expansion of equation (39) then shows that l_a must be equal to $-\frac{3}{2}$, and this yields the physically relevant solution

$$g_2 = -\frac{1}{2} - \frac{9}{2}(\tau^2 - 1) \left\{ 1 + \tau S + \frac{1}{2} [\tau + (\tau^2 - 1)S]^2 \right\}, \quad (40)$$

which behaves near $\Omega = 1$ as

$$g_2 \asymp -\frac{3}{7} \Omega^{-2/63} g_1^2, \quad (41)$$

while $g_2/g_1^2 \rightarrow -1/2$ when Ω approaches 0. The $\Omega > 1$ solutions are in [10]. The logarithmic derivative of the second order growth rate, $f_2 \equiv \frac{a}{g_2} \frac{dg_2}{da}$, behaves as $f_2 \asymp 2\Omega^{5/9}$ near $\Omega = 1$. Alternatively, it can be somewhat better approximated by $2\Omega^{4/7}$ for $0.1 \lesssim \Omega \lesssim 1$.

The third order solution is also known and was obtained in [10]. It is also separable in the $\Omega = 1$ case. But when $\Omega \neq 1$, it must be written as a sum of 2 separable pieces.

7. APPLICATIONS

Here I show how moments of the PDF can be computed in Lagrangian perturbation theory, and recover some of the result reviewed above. In particular I give the skewness for rather general non-gaussian initial conditions. Then I show how the redshift space distortion effect on skewness can be computed. Finally, I discuss using the exact perturbative solutions as approximations to the real dynamics.

7.1. Moments in the Lagrangian approach

Since the unsmoothed density contrast is given by $\delta = J^{-1} - 1$, we have

$$\langle \delta^n(\mathbf{x}) \rangle_{\mathbf{x}} = \langle (J^{-1} - 1)^n \rangle_{\mathbf{x}} = \langle (J^{-1} - 1)^n J \rangle_{\mathbf{q}}.$$

The variance and skewness are then given up to the fourth order by

$$\begin{aligned} \langle \delta^2 \rangle &= \varepsilon^2 \langle J^{(1)2} \rangle + \varepsilon^3 \langle 2J^{(1)}J^{(2)} - J^{(1)3} \rangle + \\ &\quad \varepsilon^4 \langle J^{(1)4} - 3J^{(1)2}J^{(2)} + J^{(2)2} + 2J^{(1)}J^{(3)} \rangle + \mathcal{O}(\varepsilon^5) \\ \langle \delta^3 \rangle &= -\varepsilon^3 \langle J^{(1)3} \rangle + \varepsilon^4 \langle 2J^{(1)4} - 3J^{(1)2}J^{(2)} \rangle + \mathcal{O}(\varepsilon^5), \end{aligned}$$

where all averages on the displacement field are taken with respect to the Lagrangian unperturbed coordinate \mathbf{q} .

Now consider the case of the initial density fields which can be generated by a displacement field $\tilde{\Psi}^{(1)}$ which three components are independent, with the same (but arbitrary) statistical law to insure homogeneity and isotropy. While not fully general, the generated density field $\delta_i = \varepsilon \delta^{(1)}$ encompasses a rather wide class of non-gaussian Initial conditions. We note σ_1^2 the variance of any component i of the (linear) gradient field

$$\sigma_1^2 = \langle \Psi_{i,i}^{(1)2} \rangle = \varepsilon^2 g_1^2 \langle \delta_i^2 \rangle / 3,$$

and S its third moment $S = \langle \Psi_{i,i}^{(1)3} \rangle$, and K its reduced fourth moment $K = \langle \Psi_{i,i}^{(1)4} \rangle - 3\sigma_1^4$. We thus have $\langle J^{(1)3} \rangle = 3S$, $\langle J^{(1)4} \rangle = 3K + 27\sigma_1^4 = 3K + 3\langle J^{(1)2} \rangle^2$. The other term in $\langle \delta^3 \rangle$ involves the product $J^{(1)2}J^{(2)}$ which can readily be estimated since [after (35) and (35)] we have

$$J^{(2)} = (1 + g_2/g_1^2) \sum_{i>j} (\Psi_{i,i}^{(1)}\Psi_{j,j}^{(1)} - \Psi_{i,j}^{(1)}\Psi_{j,i}^{(1)}).$$

It follows by development that $\langle J^{(1)2}J^{(2)} \rangle = 6(1 + g_2/g_1^2)\sigma_1^4$. We thus have

$$S_3 = \frac{-3S + \varepsilon g_1 6(K + 3(2 - g_2/g_1^2)\sigma_1^4)}{\varepsilon g_1 \sigma_1^4 (3 - 3\varepsilon S/\sigma_1^2)^2}. \quad (42)$$

$$= -\frac{S}{3\sigma_1^4 g_1 \varepsilon} + 4 - 2g_2/g_1^2 + 2\frac{K\sigma_1^2 - S^2}{3\sigma_1^6} + \mathcal{O}(\varepsilon). \quad (43)$$

For an initially Gaussian field with $S = K = 0$, we get the simple result

$$S_3 = 4 - 2g_2/g_1^2 + \mathcal{O}(\varepsilon^2), \quad (44)$$

whose first term corresponds to the pure Zeldovich approximation and had been found by Grinstein and Wise [27]. The value of the ratio of growing modes may be obtained

from the exact solutions given before, but it is hard to imagine practical cases when our approximation (41) might not be sufficient. We thus have the handy and quite accurate formula for a Gaussian initial field with $0.1 \lesssim \Omega \lesssim 2$ (Bouchet *et al* 1992)

$$S_3 \approx \frac{28 + 6\Omega^{-2/63}}{7},$$

which generalizes the $S_3 = 34/7$ found by Peebles (1976) in the $\Omega = 1$ case. The more general formula (43) gives the time-evolution of the skewness factor S_3 in spatially flat models for the class of non-Gaussian initial conditions which may be generated by independent displacement fields along three axes. The general formula for the $\Omega = 1$ case can be found in [24].

7.2. Redshift Space Skewness

In redshift space, the appearance of structures is distorted by peculiar velocities. At “small” scales, this leads to the “finger of god” effect: the clusters are elongated along the line-of-sight due to their internal velocity dispersion. This is an intrinsically non-linear effect, and we shall not be concerned with it. At “large” scales, the effect is reversed: the coherent inflow leads to a density contrast increase parallel to the line-of-sight. Indeed, foreground galaxies appear further than they are, while those in the back look closer, both being apparently closer to the accreting structure (Sargent & Turner 1977; LSS, §76; Kaiser 1987).

Kaiser (1987) estimated this redshift effect, in the large sample limit, on the direction averaged correlation function, and found $\langle \delta^2 \rangle^z = (1 + 2/3\Omega^{0.6} + 1/5\Omega^{1.2}) \langle \delta^2 \rangle$, where the superscript z correspond to a redshift space measurements. For $\Omega = 1$, $\langle \delta^2 \rangle^z = 28/15 \langle \delta^2 \rangle$. We now turn to a Lagrangian analysis of this effect.

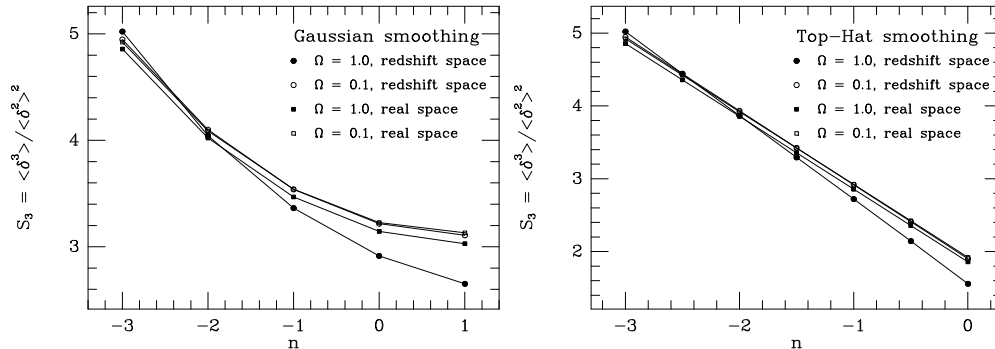


Figure 5. See legend in text. Courtesy Hivon *et al* 1993)

Let us consider the case of spherical coordinates, when distances to the observer would be estimated by means of redshift measurements. And let us now denote redshift space measurements by the superscript z . The redshift space comoving position \mathbf{x}^z of a particle located in $\mathbf{r}(\mathbf{q}) = a\mathbf{x}(\mathbf{q})$ is $\mathbf{x}^z = \dot{\mathbf{r}}/(aH)$ (with $H = \dot{a}/a$). The real space perturbative expansion (29) is then replaced by

$$\begin{aligned} \mathbf{x}^z = & \mathbf{q} + [1 + f_1(t)] g_1(t) \tilde{\Psi}^{(1)}(\mathbf{q}) \\ & + [1 + f_2(t)] g_2(t) \tilde{\Psi}^{(2)}(\mathbf{q}) + \mathcal{O}(\varepsilon^3), \end{aligned} \quad (45)$$

where we have explicitly used the separability of $\Psi^{(1)} = g_1(t)\tilde{\Psi}^{(1)}(\mathbf{q})$ and $\Psi^{(2)} = g_2(t)\tilde{\Psi}^{(2)}(\mathbf{q})$. In the limit of an infinitely remote observer, say along the r_3 -axis, we can approximate spherical coordinates by Cartesian ones. The observed density contrast δ_z in comoving coordinates is then simply $\delta^z(x_1, x_2, x_3^z)$. All we have to do, thus, is to replace everywhere in the calculation of S_3 the displacement field along the third axis

$$\Psi_3^{(m)} = g_m \tilde{\Psi}_3^{(m)} \quad \text{by} \quad (1 + f_m)g_m \tilde{\Psi}_3^{(m)}$$

for $m = 1$ and 2 . We have for instance, $\langle J^{(1)2} \rangle = [2 + (1 + f_1)^2] \sigma_1^2$.

This shows that in our so-called ‘‘infinite observer limit’’, we have $\langle \delta^2 \rangle^z = (1 + 2/3 f_1 + 1/3 f_1^2) \langle \delta^2 \rangle$ which slightly differs from Kaiser’s calculation (who did a calculation in spherical coordinates instead of our rectangular ones). Indeed, we find that the redshift space variance is boosted by a factor $30/15$ for $\Omega = 1$, instead of his value of $28/15$.

The calculation of the terms involved of the skewness calculation is fairly straightforward, with the exception of a piece \mathcal{E} which is small and can be bounded. The result for our fairly general non-gaussian model is

$$\begin{aligned} S_3^z &= 6 - \frac{(2 + (1 + f_1)^3) S}{\varepsilon (2 + (1 + f_1)^2)^2 \sigma_1^4} \\ &\quad - 2 \frac{(2 + (1 + f_1)^3)^2 S^2}{(2 + (1 + f_1)^2)^3 \sigma_1^6} \\ &\quad + 2 \frac{(2 + (1 + f_1)^4) K}{(2 + (1 + f_1)^2)^2 \sigma_1^4} \\ &\quad - 6 \frac{1 + 2(1 + f_1)^2 + (g_2/g_1^2) [3 + 2f_1 + f_2 + f_1 f_2 \mathcal{E}]}{[2 + (1 + f_1)^2]^2}, \end{aligned} \quad (46)$$

with $1 \geq \mathcal{E} \geq 0$. Of course, we recover the real space result (44) if we set $f_1 = f_2 = 0$. On the other hand, if $\Omega = 1$, we have $f_1 = 1 = f_2/2$ (and $g_2/g_1^2 = -3/7$), which yields for Gaussian initial conditions $S_3 = (35 + \mathcal{E})/7$ while, for $\Omega = 0.1$, $S_3 \approx (34.5 + 0.4\mathcal{E})/7$ (to be compared with the value of $34/7$ in real space).

The formula (46) obtained above applies only in the limit of large volumes (like Kaiser’s result), since we have taken the limit of an infinitely remote observer. A full calculation along the previous lines, but in spherical coordinates, and including the effect of smoothing, is done in [29]. In any case, equation (46) clearly shows that the ratio S_3 is, for Gaussian initial conditions, nearly independent of the value of Ω , and is barely affected by redshift space distortions. It is interesting to note, though, that in the non-Gaussian case, the distortion might be rather large, for large enough S or K .

7.3. Approach of the Non-Linear Regime

So far, we have mainly considered rigorous uses of the Lagrangian perturbative approach, for instance the derivation of a second-order quantity, the skewness of a PDF, with the help of second order perturbation theory.

Now, we examine to what extent the second-order theory brings improvement to Zeldovich approximation, when both are used as approximations to the real dynamics, i.e. outside of their rigorous validity range.

The first and second order solutions in Eulerian and Lagrangian perturbation theory were compared in [10] to spherically symmetric cases whose evolution is analytically known. For instance, the results of those approximations were checked for the density and the divergence of the velocity field in the spherical top-hat case, when its amplitude is varied. Other comparisons were made also for given smooth profiles.

Of course, direct comparisons with numerical simulations (e.g. Ref. [10] or Buchert, this volume, and references therein) were also performed. It turns out that the Lagrangian approximations perform considerably better on a given non-linear scale ℓ if they are applied to initial conditions smoothed on that scale. This avoids amplifying the small scale “noise” whose structure cannot be followed anyway.

These comparisons lead to the following approximate ranking (at least for moderate final density contrasts ~ 1):

density contrast :

Lagrangian second order > Zeldovich \gtrsim
 Eulerian second order > Eulerian linear theory,

Velocity field :

Lagrangian second order \sim Eulerian second order >
 Zeldovich \sim Eulerian linear theory.

Here the signs “>” and “ \sim ” mean respectively “more accurate than” and “of comparable accuracy to”. For relatively large final density contrasts, the Eulerian approach becomes particularly inefficient, except for the velocity field, for which it tends however to be less accurate than the Lagrangian one. The second order Lagrangian approach gives, for moderate final δ , an excellent approximation of the density contrast and the velocity field. It seems to be able to reproduce density contrasts as large as ten.

There is hope that these lagrangian approach to the non-linear regime might lead us to a better understanding of this most poorly known of all regimes, the transition between the weakly and strongly non-linear realm. It has been recently an area of considerable activity and we shall have to wait till the dust settles.

8. CONCLUSIONS

Perturbation theory already has a long and distinguished history in Cosmology, but for many years the attention focused mainly on the linear terms, *e.g.*, for early universe calculations of the power spectra of light and matter at recombination. But for the latter evolution of large scale structures, perturbation theory went out of fashion in the era which saw the advent of massive computer simulations of their formation. These allowed investigating strongly non-linear scales, the only ones that could be carefully studied statistically in the galaxy surveys of the time. Another reason of this purgatory period of the theory may have been the perception that any early signature of the weakly non-linear phase would have been totally erased by the following strongly non-linear phase, *i.e.*, that it was irrelevant. In any case, the situation has now dramatically changed, galaxy catalogs encompass ever increasing scales where density contrasts are weak; they display remarkable moments hierarchy on large scales, with a striking similarity to that observed on smaller scales. Meanwhile realistic calculations have become recently available (*e.g.*, including the smoothing inevitable in any realistic measurement, redshift distortions, etc), and last but not least, comparisons with

numerical simulations showed the predictive power of the theory. In a few years the beauty awakened, and this area of research is now striving. These notes just surveyed some of the simpler analyses, and new results are posted nearly every week. Of course, much remain to be done, and maybe the most important question to be answered is why does these perturbative approaches work so well?

References

- [1] Abramowitz, M. & Stegun, I. A., 1964, "Handbook of Mathematical Functions" (Washington: National Bureau of Standards)
- [2] Balian, R., Schaeffer, R., 1989, *Astr. Astrophys.*, 226, 373
- [3] Bernardeau, F., 1992, *Astrophys. J.*, 392, 1
- [4] Bernardeau, F., 1994, *Astr. Astrophys.*, 291, 697
- [5] Bernardeau, F., 1996, *Astr. Astrophys.*, *in press* (preprint SISSA astro-ph/9502089)
- [6] Bernardeau, F., Juszkiewicz, R., Dekel, A., Bouchet, F. R., 1996, *Astrophys. J.*, *in press* (preprint SISSA astro-ph/9404052)
- [7] Bernardeau, F., & van de Weygaert, R., 1996, *Mon. Not. R. astr. Soc.*, *in press* (preprint SISSA astro-ph/9508125)
- [8] Bouchet, F. R., Juszkiewicz, R., Colombi, S., Pellat R. 1992 *Astrophys. J.*, 394, L5
- [9] Bouchet, F. R., Hernquist, L. 1992 *Astrophys. J.*, 400, 25
- [10] Bouchet, F. R., Colombi, S., Hivon, E. & Juszkiewicz, R., 1995, *Astr. Astrophys.*, 296, 575
- [11] Bouchet, F. R., Davis, M., Strauss, M. A., Fisher, K., Yahil, A., & Huchra, J. P., 1993, *Astrophys. J.*, 417, 36
- [12] Buchert, T., Ehlers, J., 1993, *Mon. Not. R. astr. Soc.*, 264, 375
- [13] Buchert, T., 1994, *Mon. Not. R. astr. Soc.*, 267, 811
- [14] Chodorowski, M., & Bouchet, F. R., 1996, *Mon. Not. R. astr. Soc.*, *in press* (preprint SISSA astro-ph/9507038)
- [15] Coles, P., Moscardini, L., Lucchin, F., Matarrese, S. & Messina, A., 1993, *Mon. Not. R. astr. Soc.*, 264, 749
- [16] "Cosmic Velocity Fields", 1993, Proceedings of the 9th IAP meeting edited by F.R. Bouchet and M. Lachièze-Rey, Editions Frontières, Gif sur Yvette.
- [17] Cramér, H., 1946, "Mathematical Methods of Statistics" (Princeton: Princeton Univ. Press)
- [18] Doroshkevich, A. G., Ryabenkin, V. S., Shandarin, S. F., 1973, *Astrofizika*, 9, 257
- [19] Efstathiou, G., Frenk, C.S., White, S.D.M. Davis, M., 1988, *Mon. Not. R. astr. Soc.*, 235, 715
- [20] Evrard, A. E. & Crone, M. M., 1992, *Astrophys. J.*, 394, L1 *Mon. Not. R. astr. Soc.*, 235, 715
- [21] Frieman, J. & Gaztanaga, E. 1994, *Astrophys. J.*, 425, 392
- [22] Fry, J. N. 1984, *Astrophys. J.*, 279, 499
- [23] Fry, J. N. & Gaztanaga, E. 1993, *Astrophys. J.*, 413, 447
- [24] Fry, J. N. & Scherrer, R.J., 1994, *Astrophys. J.*, 429, 36
- [25] Gaztanaga, E., 1994, *Mon. Not. R. astr. Soc.*, 268, 913
- [26] Gaztanaga, E., & Yokoyama, 1993, *Astrophys. J.*, 403, 450
- [27] Grinstein, B., Wise, M. B., 1987, *Astrophys. J.*, 320, 448
- [28] Hivon, E., Paris XI PhD thesis, 1995, unpublished. 298, 643
- [29] Hivon, E., Bouchet, F. R., Colombi, S. & Juszkiewicz, R., *Astr. Astrophys.*, 298, 643
- [30] Hubble, E., 1934., *Astrophys. J.*, 79, 8
- [31] Juszkiewicz, R., Bouchet, F. R., Colombi, S., 1993a *Astrophys. J.*, 412, L9-L12
- [32] Juszkiewicz, R., Weinberg, D. H., Amsterdamski, P., Chodorowski, M., Bouchet, F. R., 1993b, *Astrophys. J.*, 442, 39
- [33] Kaiser, N., 1987, *Mon. Not. R. astr. Soc.*, 227, 1
- [34] Lahav, O., Itoh, M., Inagaki, S. & Suto, Y., 1993, *Astrophys. J.*, 402, 387
- [35] Lahav, O., Saslaw, W. C., 1992, *Astrophys. J.*, 396, 430
- [36] Lokas, E. L., Juszkiewicz, R., Weinberg, D. H. & Bouchet F. R., 1996a, *Mon. Not. R. astr. Soc.*, *in press* (preprint SISSA astro-ph/9407095).
- [37] Lokas, E. L., Juszkiewicz, R., Bouchet F. R., & Hivon, E. 1996b, *Mon. Not. R. astr. Soc.*, *in press* (preprint SISSA astro-ph/9508032).
- [38] Luo, X. & Schramm, D. 1993, *Astrophys. J.*, 408, 33
- [39] Moutarde, F., Alimi, J.-M., Bouchet, F. R., Pellat, R., Ramani, R., 1991, *Astrophys. J.*, 382, 377
- [40] Munshi, D., Sahni, V., Starobinsky, A.A., 1994, *Astrophys. J.*, 436, 517

- [41] Nusser, A. & Dekel, A., 1993, *Astrophys. J.*, 405, 437
- [42] Peebles, P. J. E., 1976, *Astrophys. J.*, 205, 318
- [43] Peebles, P. J. E., 1980, "The large Scale Structure of the Universe" (Princeton: Princeton Univ. Press) astro-ph/9505005 [abs, src, ps] :
- [44] Sahni, V. & Coles, P., 1995, Phys. Rep., in press, (preprint SISSA astro-ph/9505005)
- [45] Sargent, W. L. W. & Turner, E. L., 1977, *Astrophys. J.*, 212, L3
- [46] Scoccimarro, R. & Frieman J., 1996, preprint (Fermilab-Pub-95/292-A and SISSA astro-ph/9509047)
- [47] Strauss, M. A. & Willick, J. A., 1995, Physics Reports, 261, 271, *in press* (preprint SISSA astro-ph/9502079)
- [48] Weinberg, D. H. & Cole, S., 1992, *Mon. Not. R. astr. Soc.*, 259, 652
- [49] Zeldovich, Ya., B. 1970, *Astr. Astrophys.*, 5, 84